Proceedings of PVP2008
2008 ASME Pressure Vessels and Piping Division Conference
July 27-31, 2008, Chicago, Illinois, USA

PVP2008-61853

THERMAL FATIGUE CYCLIC-DOWN SHOCKS ON 316L MODEL PIPE COMPONENTS

Elena Paffumi
Institute for Energy, Joint Research Centre
P.O. Box 2, 1755 ZG Petten, The Netherlands

Karl-Fredrik Nilsson
Institute for Energy, Joint Research Centre
P.O. Box 2, 1755 ZG Petten, The Netherlands

Nigel Taylor
Institute for Energy, Joint Research Centre
P.O. Box 2, 1755 ZG Petten, The Netherlands

ABSTRACT

There is a continuing need for reliable thermal fatigue analysis tools to ensure that high safety levels are maintained in the main coolant lines of light water reactors. To advance the accuracy and reliability of thermal fatigue load determination, a combined experimental and numerical investigation has been conducted on cylindrical components of 316L stainless steel subjected to cyclic thermal shocks of varying intensity. Slightly different experimental conditions were applied in each test to explore the effect of ΔT_{max} values of increasing severity, the effect of a superimposed static axial load and a reduced test piece wall thickness.

Particular attention is given in this work to the influence of a constant tensile axial load on the quenching down shock damage. A comparison between thermal down-shock tests with and without additional constant tensile load is analysed in details here below.

INTRODUCTION

Thermal fatigue is a widely recognised important potential damage mechanism in cooling piping systems of light water reactors [1,2] and its significance increases as plants get older, requiring safety justifications for up to 60 years of operation. Feature tests i.e. tests involving simulated thermal fatigue performed under laboratory conditions on test pieces with component relevant geometries, play an important role in the verification of assessment procedures and for establishing transferability of standard fatigue curves to component-life situations. Several series of tests have been performed in Europe in recent years [3,4,5,6] but few provide crack growth data.

The European Commission has also supported research in this area via the THERFAT project [7], which ended in 2004 and produced a road-map for development of a European thermal fatigue evaluation methodology. This challenge has been taken further in the NESC Thermal Fatigue project [8] and NULIFE European network of excellence project.

To improve the knowledge in this respect and contribute to the development of improved methods for assessing possible thermal fatigue damage in nuclear plant piping systems, a unique set of crack growth data has been generated for tubular test pieces in 316L(N) stainless steel subjected to cyclic thermal loads in a specially designed rig [9,10,11,12,13].

MATERIAL PROPERTIES

The specimens used for the study were machined from 316L(N) stainless steel plate of thickness 60 mm. The physical and mechanical properties of this class of steel have been extensively characterised. For the plate used in the present study, a limited series of low cycle fatigue tests were performed at ambient temperature; the results confirmed that the properties of the plate are consistent with reference curves in the RCC-MR code [14]. Consequently, the RCC-MR curves over the temperature range of interest in this study (25 to 400^{o}C) were used in the analysis work.

For fatigue crack growth, the Paris law coefficients derived from data in the review by Huthmann and Picker [15] are used:

$$\frac{da}{dN} = 2.67x10^{-10}\left(\Delta K\right)^{3.89} \qquad \text{Eq. (1)}$$

where the units of K are MPa.√m and a is in mm.

EXPERIMENTAL SET-UP

The thermal shock experiments are carried out on cylindrical specimens in a special test facility (Fig. 1). The test piece consists of a tubular section of outside diameter of 48 mm, 14 mm wall thickness and an overall length of 224 mm. During a test the outer surface temperature is maintained constant (typically at 300°-400°C) by induction heating while the bore is subject to repeated quenching with room temperature water. The overall cyclic frequency was approximately 0.02 Hz. The imposed outer surface temperature determines the severity of the cycles. During the cycling the test piece is held in a lever arm test machine, which allows application of a static axial load, but places no restraint on axial displacement. The induced cyclic thermal stresses typically cause the initiation of a network of cracks at the inner surface; some of these then propagate further into the wall thickness. The application of static axial load on the specimen is used to study the influence of pressure and system loads on the thermal fatigue damage development (particular attention will be given to these tests in this work). In PWR systems the pressure at a given location is nominally static during operation, with hoop stresses of the order of 50 MPa. This is expected to have little effects on crack initiation, but may be relevant for crack propagation.

A summary of the experimental conditions for the six tests performed so far is given in the Table 1. Attention will focus in this work on tests TF1(300°C) and TF4(300°C+50kN) as explained above. The values for the imposed duration of the quenching shock t_{Quench} and of the up-shock without water t_{Heat} were of 5 and 40 or 5 and 45 seconds respectively, implying an overall cyclic frequency of approximately 0.02 Hz. The tensile load of 50kN and 100kN corresponds to a nominal section stress on the specimen of 33MPa and 66MPa respectively.

The tests were interrupted periodically to allow the non-destructive measurements. In the initial phase of each test, surface replica measurements were made to detect initiation, a rather difficult process due to the space restriction imposed by the 20 mm bore diameter, the diffuse nature of the surface damage and the need to make three 120° replicas in order to check the entire inner circumference. Table 1 includes the cycles to initiation value as determined from the replica measurements.

Once it has been established in this way that initiation had occurred, a non-destructive ultrasound time of flight diffraction technique (TOFD) with a resolution of ±0.5 mm was applied to follow the growth of the network of cracks [11]. This required a complete scan of the specimen, followed by identification and then sizing of the cracks (which could be up to or more than 10 for each specimen). During the successive test stops, the same scanning and sizing procedure was repeated to follow the crack growth. It is noted that crack lengths were difficult to determine with any precision and such values were therefore not systematically collected. Typical results for crack lengths and depth distributions from TOFD inspections are shown in Fig. 2a) and b).

Fig. 3 shows plots of the crack depth measurements for individual cracks for TF1 and TF4 specimens as a function of thermal shock cycles. In the case of TF1, the test was run for 55000 cycles before the first interruption for damage measurements. It was established that initiation had already occurred (one crack was 2.2 mm deep). As a result, the subsequent tests were interrupted earlier.

Overall the development of cracking appears take place in two stages. First a network of surface cracks develops. In the second phase a few cracks (axial as well as circumferential) propagate, but at a non-uniform growth rate, with apparently stable periods follow by renewed crack growth in some instances. This behaviour is possibly influenced by complex interaction or crack closure effects. It is also noted that measurement of this type of damage, involving a distributed field of shallow cracks, is at the limits of the resolution of the TOFD system (±0.5 mm).

In Fig. 3 it can be noted that the number of cracks is higher in the case with additional axial load; this difference increases with increasing number of cycles. More circumferential cracks are detected than axial cracks, as expected due to the presence of the tensile load. These aspects are depicted in Fig. 4, which shows a comparison between the number of circumferential and axial cracks in function of number of quenching cycles, as from TOFD inspections, for both tests TF1 (300°C) and TF4 (300°C+50kN). It can be also noted that the number of axial cracks for the test TF1 without axial load is slightly higher compared to that of the circumferential cracks and this aspect can be supported from the comparison of ΔK values for both cases as shown later in Fig. 7 (the cracks are deeper than 2mm).

To provide a better comparison of behaviour under different test conditions, crack growth rates were calculated for each individual crack by a simple linear fit between adjacent data points. In general, for thermal loading conditions an initial increase in growth rate would be expected as the crack grows into the wall thickness, followed by a decrease as the thermal stress reduces further into the section. Fig. 5 plots such data as a function of crack depth for the TF1 (300°C) and TF4 (300°C+50kN) tests. Considerable scatter is evident. In the case of the test TF4 some damage (cracks of slightly less than 1 mm depth) was detected in the first inspection stop after just 10000 cycles, indicating that the initiation had occurred at this point. The test TF4 has been run to 104000 cycles in total. Both data sets show similar trends up to date; there is some evidence suggesting that crack growth rate is slightly higher in the initial stages of the test with additional axial load.

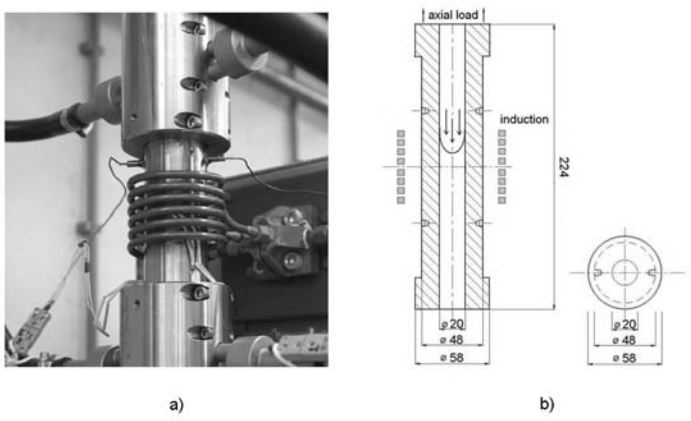

Fig. 1 Experimental set-up a) specimen with induction coil b) specimen dimensions.

Test	t_{Quench} /t_{Heat} (sec)	T_{max} (ºC)	T_{water} (ºC)	N_i	Total Cycles to Date
TF1	5/40	300	25	≤55600	200000
TF2	5/45	400	25	14700-20000	47000
TF3	5/45	350	25	15000-20000	30000
TF4	5/45	300 +50kN	25	10000	104000
TF5	5/20	400	25	≤10000	65000
TF6	5/45	300 +100kN	25	NA	10000

Table 1: Thermal fatigue test summary.

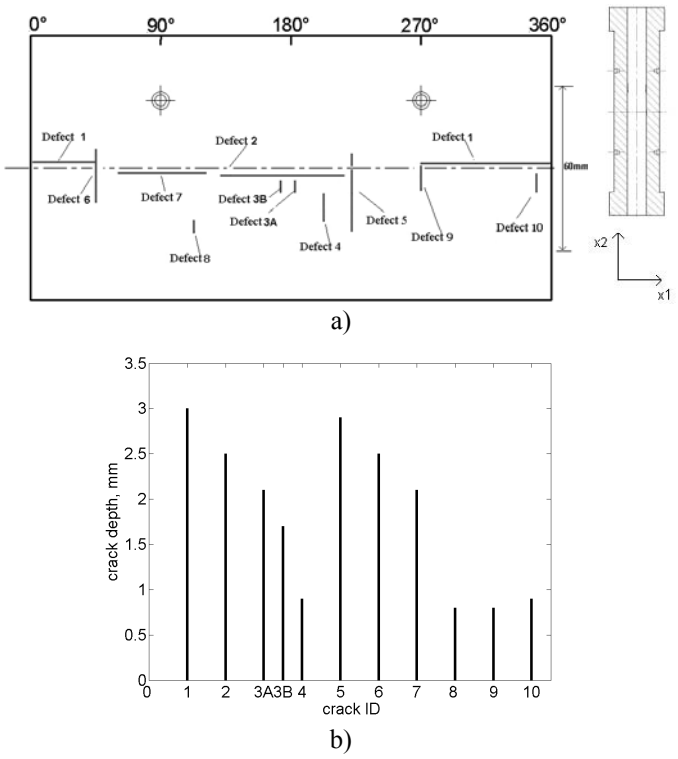

Fig. 2 Orientation, location and length of defects in TF1 (300ºC) after 90000 cycles from TOFD measurements a) and depth distribution b).

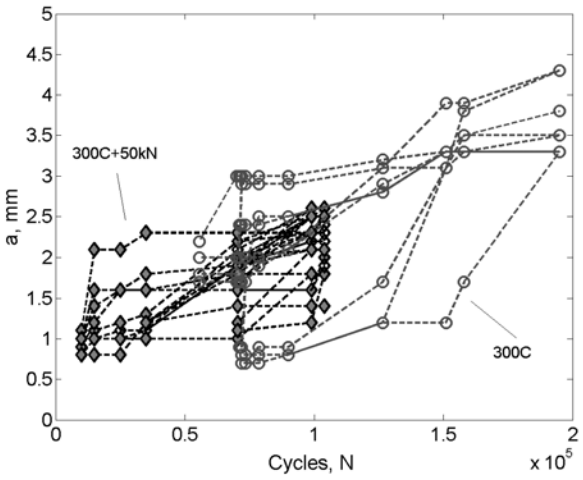

Fig. 3 Crack depth data versus number of quenching cycles for the tests TF1 (no additional axial load - o) and TF4 (with an axial tensile load of 50kN - ◊) for the thermal shock cycle with Tmax = 300°C.

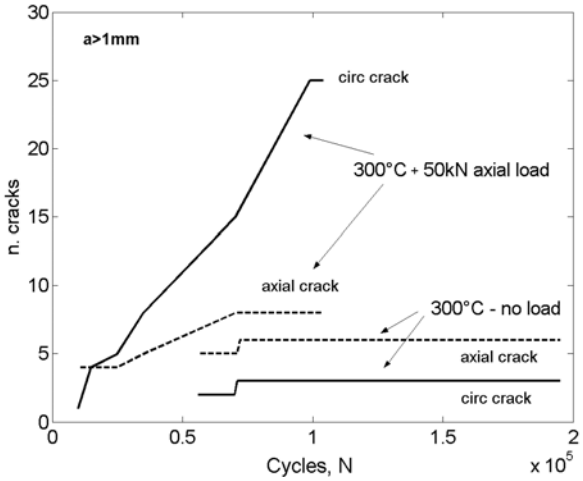

Fig. 4 Comparison between the number of circumferential and axial cracks versus number of quenching cycles for tests TF1(300°C) and TF4(300°C+50kN).

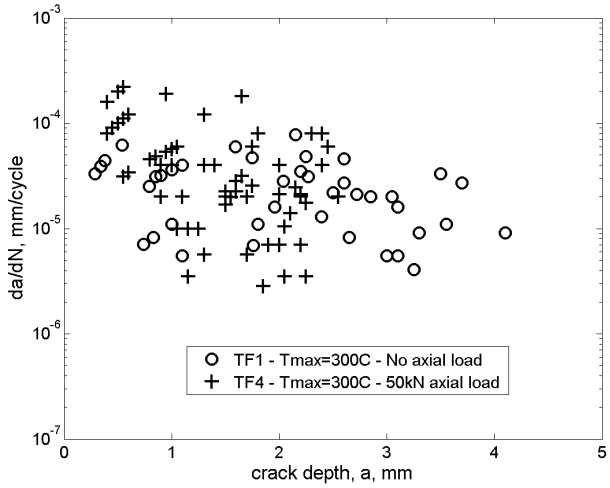

Fig. 5 Crack growth rate versus crack depth for the tests TF1 (no additional axial load) and TF4 (with an axial tensile load of 50kN) for the thermal shock cycle with T_{max} = 300°C.

FINITE ELEMENT MODEL

Finite element simulations using the commercial code ABAQUS were used to perform uncoupled thermal stress analysis of the cycle applying the resulting temperature fields to determine the thermal stresses and strains [9]. Symmetry was assumed and only the upper half of the specimen needed to be modelled. Auxiliary software routines were developed to automatically generate finite element meshes with a progressive mesh refinement towards the inner surface to capture the large strain variations induced by the thermal shocks. The mechanical and thermal boundary conditions, in particular the adopted function for the heat transfer coefficient *h* [9], were fine-tuned by comparison between the numerical predictions and the temperatures measured on specially prepared calibration specimen equipped with six thermocouples across the wall. The mechanical boundary conditions and strain numerical predictions were calibrated by mean of high temperature strain gage measurements.

The temperature dependent thermal expansion coefficient, α, and Young's modulus, E, were used together with the non-linear kinematic hardening model proposed by Lemaitre and Chaboche [16], which was implemented in ABAQUS [10]. The model parameters were calibrated from the RCC-MR cyclic stress-strain curve for 316L as functions of the applied strain range [10] and were selected during the analysis in relation to the strain range variation at each integration point of the FE elements by mean of a dedicated user-subroutine. For each T_{max} cycle the model was run for 10 full cycles to allow shakedown to a stabilised response.

FRACTURE MECHANICS ANALYSIS

Prediction of crack growth typically relies on first estimating the stress intensity factor range (ΔK) for the postulated crack geometry and using a Paris-type fatigue crack growth law to arrive at a crack growth rate. In the present case two approaches to determining ΔK have been examined. The first is a so-called engineering approach using analytical formula in conjunction with the cyclic thermal stress profiles generated from a FE un-cracked body analysis. The second uses 3-D FE cracked-body analysis [13]. In both cases the defect geometry treated is that of a single sharp semi-elliptic crack on the inner surface of the test piece, with either an axial or circumferential orientation.

Analytical Approach

Following an approach widely used in the nuclear industry for assessing postulated defects [17,18,19], the stress intensity *K* at a postulated semi-elliptical crack (axial or circumferential) of depth *a* (Fig. 6) can be estimated via the use of influence functions [20]:

$$K = \sqrt{\frac{\pi a}{Q}}\left[b_0 i_0 + b_1 i_1 \frac{x}{t} + b_2 i_2 \left(\frac{x}{t}\right)^2 + b_3 i_3 \left(\frac{x}{t}\right)^3 \right] \qquad \text{Eq. (2)}$$

Where:

-*x* is a variable originating at the inner surface indicting the distance across the wall thickness, *t*;

-b_0, b_1, b_2 *and* b_3 are coefficients for the polynomial expression:

$$\sigma = b_0 + b_1 \frac{x}{t} + b_2 \left(\frac{x}{t}\right)^2 + b_3 \left(\frac{x}{t}\right)^3, \qquad \text{Eq. (3)}$$

which fitted to the stress distribution through the wall thickness for $0 \le x \le a$;

-i_0, i_1, i_2 and i_3 are influence coefficients which depend on the crack/thickness ratio, *a/t*, on the shape of the crack, *a/c*, and on the location along the crack front, and are given by handbook solutions [20,21];

-Q is a shape correction factor, defined for a semi-elliptical crack as [20]: $Q = 1 + 1.464\left(\frac{a}{c}\right)^{1.65}$.

Values of K were calculated using the above so-called analytic method (since the influence coefficients were themselves derived from 3-D cracked body linear elastic FE analyses) for various crack geometries and orientation using polynomial fits to the appropriate stress distributions i.e. of the stress component in the direction perpendicular to the plane of the crack, for different time steps during the thermal shock cycle. Although the approach is in principle elastic, it was also applied using the stress distributions from the 2-D elasto-plastic analyses to assess if this would provide a simple means of obtaining less conservative predictions than from the purely elastic approach. Formulas and experimental results data are often derived for stress-controlled conditions and for constant loadings. In thermal fatigue, the loading is essentially strain-controlled and with large through thickness stress gradients, hence an elastic analysis is conservative. It is noted that [21] provides values of the coefficients i_0, i_1, i_2 and i_3 for cylinder with a wall thickness/inner radius ratio, t/r_i, of up to 1.0; these t/r_i =1 values were used here, even though the test pieces have a higher value of $t/r_i \approx 1.4$. The K_{max} and ΔK estimates could be obtained at different locations along the crack front, from surface to deepest points, for any crack dimension in either the circumferential or axial orientations. It is noted that the values of the surface point are always a bit questionable since there is a vertex "double singularity".

Fig. 7 compares the maximum values of K calculated at the deepest point for a circumferential and an axial defect under the T_{max}=300°C thermal cycles and for a crack aspect ratio equal to *c/a*=4. As expected the K values determined from the elasto-plastic stress distributions are much lower than those from the elastic stress distributions. Another difference lies in the crack depth at which K is at its maximum: for instance with the T_{max}=300°C cycle, the K value peaks for a crack depth of 2.2 mm with the elastic stress distribution and at a=4.7 mm for the elasto-plastic stress distribution. This is expected since the stress concentration at the free surface is greater for the elastic case. It is also noted that the difference between axial and circumferential crack K values is very small. This is in line with the observations that axial and circumferential cracks grow at similar rates (see for instance Defect 6 and 7 in Fig. 2), but the axial cracks are slightly higher in number as shown before in Fig. 5. Working from these relationships of K with crack depth, crack growth predictions are made using the Paris fatigue crack growth law. The stress intensity range is given by ΔK_{eff}, where the subscript "eff" stands for "effective", so that only the part of the cycle when the crack remains open should be accounted for. For the type of thermal loading cycle analysed here, if K_{min}<0, then K_{min} is taken as zero, so that $\Delta K_{eff} = K_{max}$ and R=K_{min}/K_{max}=0. The integration procedure requires additional assumptions about the shape of the crack, in particular the aspect ratio, *a/c*, which influences the value of K via the crack shape expression Q.

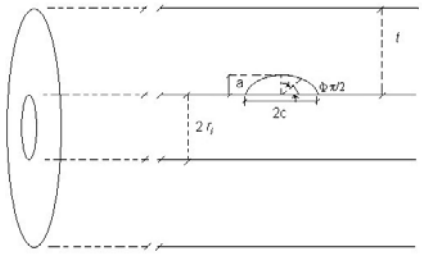

Fig. 6 Schematic representation of an internal axial surface crack in a cylinder.

3D Cracked-Body Analysis

The 3-D finite element simulation of surface cracks was undertaken because there was a need to verify the ΔK estimates calculated by the engineering approach described above in relation to factors such as: the effect of the cyclic plasticity model, the high t/r_i ratio of the test piece, the mixed stress/displacement controlled loading conditions and the significant surface plasticity induced by the thermal shock. Previous work by the authors [10,12] therefore explored the use of a crack tip opening displacement (denoted here as CTOD or δ) parameter for a 2-D axisymetric configuration i.e. a fully circumferential crack, and converted this to the ΔK_δ for application of the fatigue crack growth law. Δδ is taken as the maximum range of δ during a cycle, in which δ is set to zero if the computed opening becomes negative. The value of δ was then converted to a K_δ estimate using the relation between δ and J originally proposed by Shih [22] and the plain strain relation between K and J:

$$\Delta K_\delta = \sqrt{\frac{\sigma_0 \cdot E}{d_n(1-\nu^2)}}\left(\sqrt{\delta_{max}} - \sqrt{\delta_{min}}\right) \qquad \text{Eq. (4)}$$

where σ_o is the yield stress, d_n depends on the hardening and the ratio σ_o/E, E is the Young's modulus and v is the Poisson's ratio.

This approach is also considered here for the 3-D crack configuration, which is more relevant to practical applications in which damage is typically localised to a segment of the pipe circumference. The values of δ were computed directly from the crack opening profile given by the 3-D FE analysis as the crack opening at the ±45° line from the crack tip [13,22]. It is noted that δ was verified to be always positive during a cycle.

It should be pointed out that this procedure has a number of approximations. First of all there is obviously some mesh dependence but due to the convergence problems a systematic mesh refinement could not be performed for the elliptical crack. A mesh sensitivity analysis was performed for an axisymmetric crack in [13].

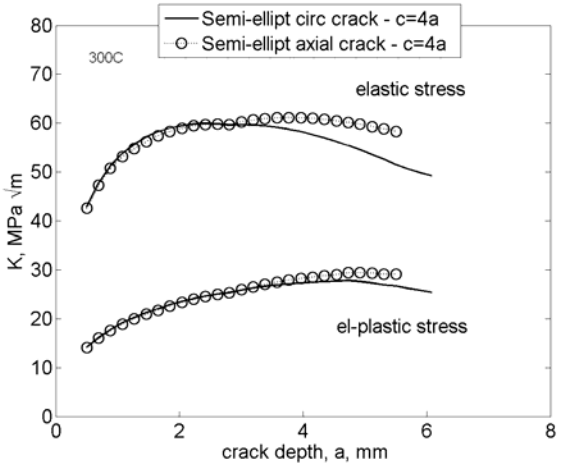

T_{max}=300°C, c/a=4

Fig. 7 Comparison the maximum K values predicted from the analytical formula for a semi-elliptic circumferential and axial crack of increasing depth under the thermal shock cycle with Tmax=300˚C for crack shape ratios of c/a=4.

ANALYSIS AND DISCUSSION

The initial focus for the comparison between the predictions and the experimental data was the dependence of crack growth rate on crack depth. Fig. 8 compares predictions from the analytic *K* model based on elastic stresses (A-E) and analytic *K* model based on elasto-plastic stresses (A-EP) models with the data for thermal cycling tests with T_{max} values of 300°C and with and without axial load of 50kN.

In Fig. 8a) the A-E and A-EP curves were calculated for a fixed value of crack shape ratio (*c/a* equal to 16 [23]). In this plot the effect of the axial load of 50kN and 100kN is visible for crack deeper than 3mm. The higher the load, higher is the effect on the crack driving force. Additional experimental cycles are requested to be able to collect further crack depth data to support this prediction (a<3mm so far for TF4 (300°C+50kN)). For this study, as an alternative to assuming a fixed value of *c/a*, a procedure was devised that allows the ratio to increase i.e. the crack grows more lengthwise than in depth. Initially a 1 mm deep defect is assumed. Iterative calculations are then made to find a value of c that gives $\Delta K_{surface} = \Delta K_{deep}$. In the subsequent step the crack depth is incremented by Δa, and the process of finding a new c value to give $\Delta K_{surface} = \Delta K_{deep}$ is repeated. In Fig. 8b) the A-E and A-EP curves were both derived using this variable c/a procedure. The computed *c/a* ratio increases with a. For a values equal to 1 and 6 mm, the respective *c/a* ratios to give $\Delta K_{surface} = \Delta K_{deep}$ were about 2 and 4 for the elasto-plastic case. Because of concerns that the near-surface plasticity was unduly affecting the results, this procedure of *c/a* ratio calculation was checked using a K value at different locations between the deepest and surface points along the crack front (i.e. 45 and 60˚ with respect to the surface line).

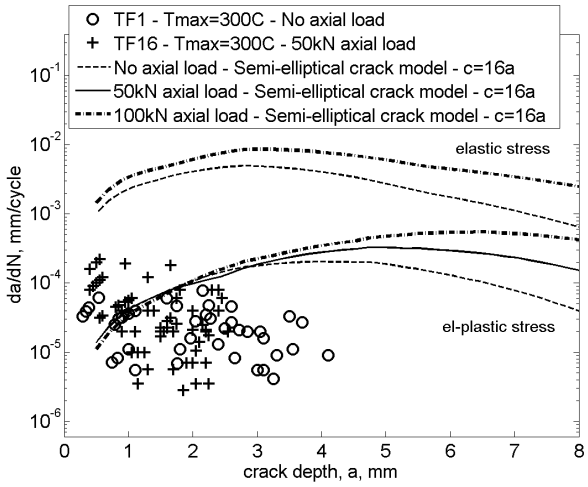

a)

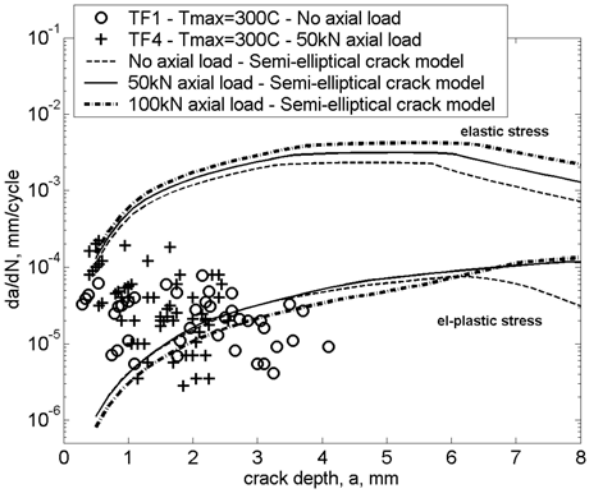

b)

Fig. 8 Influence of an additional axial load on crack growth rate for thermal fatigue cycling with Tmax = 300ºC;the predictions are from the engineering model for a semi-elliptical defect of initial depth 0.5 mm for a) a fixed aspect ratio of c=16a and b) variable *c/a*.

The results are however very similar. The TOFD measurements also showed *c/a* values increasing with depth, ranging from about 3 to 10, Fig. 2, for the first part of the test.

Considering the predicted influence of an additional constant tensile load on the crack growth rate, it can be noted from Fig. 8b) that this is reduced in comparison with that evident in Fig. 8a) with a fixed *c/a.* This is due to the change of the *c/a* ratio and the fact that the effect of the load at the surface is smaller. Fig. 9 shows the computed values of *c/a* versus the crack depth for the three cases (300˚C, 300˚C+50kN and 300˚C+100kN) for the A-EP model. The *c/a* ratio increases more slowly with increasing crack depth for the cases with load in comparison to that without axial load. Deep crack depths

(>6mm) need to be reached before the effect of the load becomes evident, both for 50kN and 100kN; this has to be verified experimentally. This reflects the modest contribution of the load to *K* (ranging from 2 to 5 MPa.√m for crack depths of 1 to 4 mm and load of 75kN) in particular in the first phase of the crack growth. The cracks tend to grow to the same depth and acceleration could be expected when this condition is reached at different locations along the circumferential extension on the inner surface. In contrast, as noted above, there is some evidence that the crack growth rate was higher in the test with the additional load, at least for the initial stages of growth.

Overall Fig. 8 shows that, as expected, the A-E model strongly over-predicts the crack growth rate and, while potential useful for providing conservative assessments, it is not discussed further here. On the other hand the A-EP models for the Tmax = 300°C thermal cycles underestimate the measured values for crack depths less than 2 mm (which is expected due to short crack effects), but predict more realistic rates for deeper cracks, although not predicting the decrease of the crack driving force through the wall thickness. In general these predictions are very sensitive to the assumed Paris law coefficients. Fig. 10 shows the effect of using the Paris law values from the A16 code [14] for the Tmax=300°C thermal loading cycle. The resulting prediction is seen to provide an upper bound to the data, without the apparently excessive conservatism of the purely elastic approach.

Whereas the experimental crack growth rates show no clear dependence on crack depth, the A-EP models predict a progressive increase of growth rate up to crack depths of at least 4 mm. Fig. 10 also gives predictions from the 3-D CTOD (ΔK_δ) method and shows how these seem to better predict the decrease of the crack growth rate with increasing crack depth.

Finally, Fig. 11 and Fig. 12 illustrate the predicted crack depths as a function of thermal cycles for the T_{max}=300°C and the T_{max}=300°C+50kN tests respectively. The starting condition of the integration is a crack of 1 mm depth at the number of cycles corresponding to initiation. The curves underline the strong conservatism of the predictions based on elastic stresses. The fact that the A-EP models underestimate the crack growth in both cases is due to the assumed "best-estimate" Paris law coefficients and conservative predictions are obtained if the upper bound A16 coefficients are introduced. Predictions based on the ΔK_δ distributions from the 3-D FE analyses are also included, indicating that changing the assumed crack aspect ratio from *c/a*=2 to *c/a*=4 can lead to a reduction in the number of cycles to reach a given crack depth and with a generally better description of the global crack growth behaviour.

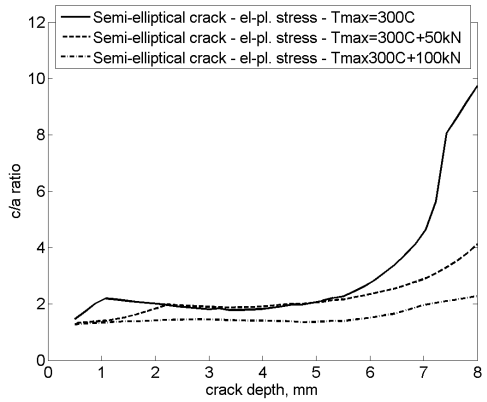

Fig. 9 Shape ratio *c/a* versus crack depth from the semi-elliptical analytical model for Tmax=300˚C, Tmax=300˚C+50kN and Tmax=300˚C+100kN.

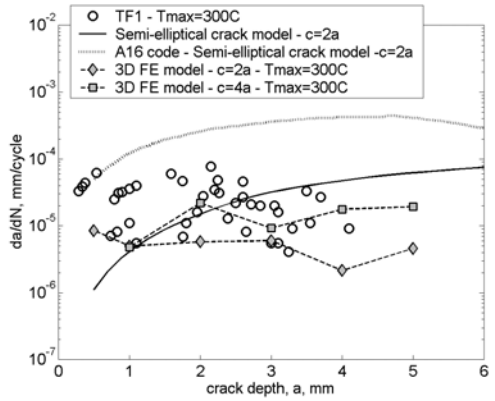

Fig. 10 Influence of the assumed Paris Law on the crack growth rates predicted by analytical model with elasto-plastic stresses for semi-elliptical defects with *c/a*=2.

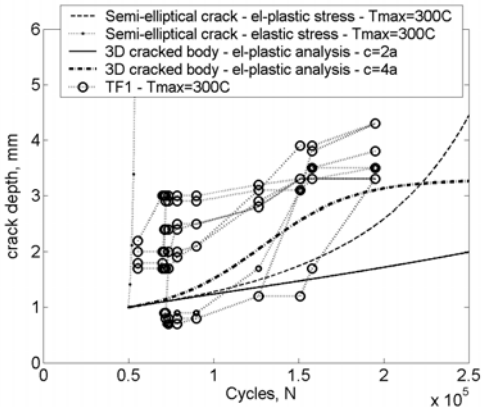

Fig. 11 Comparison of the predicted crack growth curves for circumferential defects with the experimental data for the TF1 test (T_{max}=300°C, no axial load).

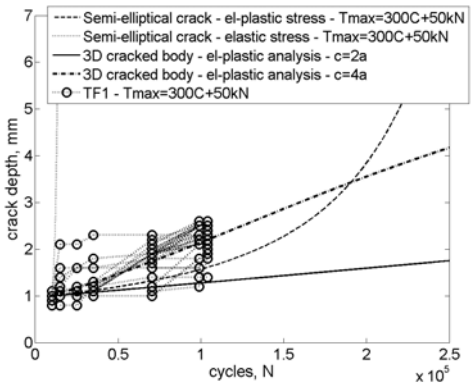

Fig. 12 Comparison of the predicted crack growth curves for circumferential defects with the experimental data for the TF4 test (T_{max}=300°C, 50kN axial load).

CONCLUSIONS

- A series of five cyclic thermal fatigue tests have been carried out on tubular specimens in 316L(N), with test durations of up to 200000 cycles. Slightly different experimental conditions were applied in each test to explore the effect of a superimposed static axial load. The surface replica technique was used to check for crack initiation. By the application of the TOFD technique a unique set of crack depth vs. number of cycles data is available for verification of damage models.
- For prediction of the growth of semi-elliptical surface cracks under thermal fatigue, the use of an analytical method based on handbook *K* solutions for elastic stress distributions produces overly conservative estimations. Applying the same method using the elasto-plastic stress distribution and the A16 Paris law gave predictions that bounded the experimental data.
- The models predict little effect of the superimposed axial load for crack depth less than 2mm. The limited experimental data suggests some effect in accelerating initiation and in the short crack growth rate; this aspect needs further investigation. An increasing rate could be expected with increasing of the depth of the cracks. Additional experimental data are requested to be able to support this prediction.
- The present single-crack fracture mechanics approaches appear to overestimate the crack growth rate with increasing crack depth; further work is needed to better model these effects and potentially reduce conservatism, addressing for instance crack closure and multiple crack interaction.

ACKNOWLEDGMENTS

The authors gratefully acknowledge the support to the experimental work given by technical staff at the Institute of Energy.

REFERENCES

1. IAEA, "Assessment and management of ageing of major nuclear power plant components important to safety. Primary piping in PWRs", TECDOC-1361, July 2003
2. C. Faidy et al, Thermal Fatigue of Reactor Components in OECD-NEA countries: a Three-fold Program to Enhance cooperation, Proc. SMiRT-18, Beijing, China, August 2005
3. FAT3D – An OECD/NEA benchmark on thermal fatigue in fluid mixing areas, Report No. NEA/CSNI/R(2005)2, 2005
4. F. Curtit et al, INTHERPOL thermal fatigue test, NEA/CSNI/R(2004)21, Proc. 3rd Int. Conf. on Fatigue of Reactor Components, Seville, Spain, October 2004
5. V. Maillot, PhD Thesis in French, Ecole Centrale de Lille, Univ des Sc de Tech de Lille. CEA report R – 6041 (2003)
6. K. Calonius and J. Solin, "Case Study on Thermal Fatigue Potential in a T-Joint", Proc. 3rd Int. Conf. on Fatigue of Reactor Components, October, 2004, Seville, Spain
7. K.-J. Metzner & U. Wilke, European THERFAT project—thermal fatigue evaluation of piping system "Tee"-connections, Nuclear Engineering & Design, Vol.. 235, Issues 2-4, 2005, 473-484
8. N. Taylor, K.F. Nilsson, M. Dahlberg, C. Faidy, A procedure for thermal fatigue damage assessment due to turbulent mixing in nuclear piping systems, Proc. Int. Conf. "Fatigue Design", Senlis, November 2005
9. E. Paffumi, Simulation and Modelling of Thermal Fatigue Damage in Austenitic Piping Components, Ph.D. Thesis, Univ. of Swansea, UK, 2004
10. Paffumi E., Nilsson K-F, Taylor N., Hurst R. and Bache M. R., Cracks initiation, propagation and arrest in 316L model pipe components under thermal fatigue, *J. ASTM International*, May 2005, Vol.2 No.5
11. Paffumi E., Nilsson K-F, Taylor N., Hurst R. and Bache M.R., Measurement of shallow crack growth during thermal fatigue of 316L tubular test piece, Proc. 3rd Int. Conf. *Fatigue of Reactor Components*, OECD/EPRI Seville, 3-6 October, 2004
12. E. Paffumi, K. F. Nilsson, N. G. Taylor, *Analysis of the Thermal Fatigue Cracking of 316L Model Pipe Components Under Cyclic Down-Shocks*, Proceeding of ASME – Pressure Vessels and Piping Division Conference 2005, Technologies for Safe and Efficient Energy Conversion, Vol. *Design and Analysis of Piping Components, Thermal Stresses and CFD in Vessel Design*, edited by J. McCabe July 17-21, 2005, Denver, Colorado, USA

13. E. Paffumi, K.-F. Nilsson, N.G. Taylor, Simulation of Thermal Fatigue Damage in a 3156L Model Pipe Component, Under revision in *Int. Journal of Pressure Vessel and Piping*, *Submitted April 2007*
14. RCC-MR Design and Construction Rules for Mechanical Components of FBR Nuclear Islands and High Temperature Applications, Tour Framatome, 2007 Edition
15. Huthmann H. and Picker C., Behaviour of short fatigue cracks in austenitic stainless steels literature review, European Commission, *Nuclear Science and Technology*, EUR 15186.
16. Lemaitre J. and Chaboche J-L, *Mechanics of Solid Materials,* Cambridge University Press, Cambridge, UK, 1990.
17. ASME, Code case N-201-4, Appendix Y
18. ASME Nuclear Boiler and Pressure Vessel Code – Section XI – ASME 2004
19. Régles de surveillance en exploitation des matérials mécaniques des ilots nucléaires REP, RSE-M edition 1997.
20. I.S. Raju, J. C. Newman Jr., Stress-Intensity factors for internal and external surface cracks in cylindrical vessels, Journal of Pressure Vessel Technology, Vol. 104, pp. 293-298, 1982
21. Chapuliot S., Formulaire de K_I Pour les Tubes Comportant un Defaut de Surface Semi-elliptique Longitudinal ou Circonferentiel, interne ou externe, Direction de l'information scientifique et technique, CEA/SACLAY-R-5900, France, ISSN 0429 3460, 2000
22. Shih C.F., "Relationships between the J-integral and the crack opening displacement for stationary and extending cracks," J. Mech. Phys. Solids, Vol. 29, No. 4, 1981, pp. 305-326.
23. Fatigue Crack Flaw Tolerance in Nuclear Power Plant Piping. A basis for Improvements to ASME Code Section XI Appendix L – NUREG/CR-6934 PNNL-16192